Proceedings of ICRC 2001: 4116 © Copernicus Gesellschaft 2001

ICRC 2001

Trapped protons with R>400 MV in near Earth belts with the AMS experiment

G. Esposito, E. Fiandrini, B. Bertucci, B. Alpat, R. Battiston, W.J. Burger, G. Lamanna, and P. Zuccon

University and INFN of Perugia

Abstract. Accurate measurements of proton fluxes at rigidities above 400 MV have been performed by the Alpha Magnetic Spectrometer (AMS) at altitudes of 370-390 Km and in the geographic latitude interval $\pm 51.7^o$. We present an analysis of the AMS data, focused on the study of the magnetically trapped component of these fluxes. The flux maps as a function of the magnetic variables (L,α_o) are determined in the interval $0.95 < L < 3$, $0^o < \alpha_o < 90^o$ for protons with R<10 GV. The results are compared with existing data at lower rigidities and in similar (L,α_o) range.

1 Introduction

For the low altitude (250-1000 Km) region near the Earth, where human activity, both commercial as well as scientific, has greatly increased over the last decade, it is particularly important to accurately model the radiation environment. Measurements carried out since the 1950s have shown the existence of radiation belts, containing energetic particles trapped in the Earth's magnetic field. Protons constitute the dominant part of this trapped population. A coarse separation can be made between trapped particles with mirror heights above 100 Km, the *stably trapped* component, weakly interacting with the upper atmosphere, where the fluxes are very intense and particles with lower mirror heights, the *albedo* component, strongly interacting with the atmosphere, not stably trapped and with less intense flux. At low altitude the stably trapped component can be observed only over the South Atlantic Anomaly (SAA) where the inner radiation belts come closer to the Earth. Outside of it, only the albedo component can be observed. A large effort has been done to accurately model the stably trapped component and the currently available models are the AP8 [(Sawyer, 1976)] and INP [(Getselev, 1991)]. These models, based on satellite experiments, cover the energy range 0.1-1000 MeV. However, no comprehensive high energy measurements of the albedo spectrum exist. The flux intensity for secondary protons created in nuclear interactions of primary cosmic ray particles was calculated under simple hypothesis in Ray (1962), but in this case a complete MonteCarlo model does not exist. No accurate measurements were available for the composition and flux intensity in the near Earth region in the rigidity range 0.4-10 GV until the AMS flight in 1998. In the following, we will use the high statistics collected by the AMS experiment in 1998 to present a detailed study of under-cutoff proton fluxes in the O(10 GV) rigidity region. They are analyzed in terms of the canonical invariant coordinates of the particles motion, the L parameter, the equatorial pitch angle with $\boldsymbol{B}$ field, α_0, and the mirror field B_m [(McIlvain, 1961), (Hilton, 1971)].

Correspondence to: G. Esposito
(gennaro.esposito@pg.infn.it)

2 AMS and the STS-91 flight

AMS is a large acceptance device designed to operate on the International Space Station (ISS) for an observational period of three years. A prototype version of the detector (average acceptance $\sim 0.16\,\mathrm{m^2 sr}$) was built in 1998. The detector was based on a high resolution silicon tracker providing an analyzing power of $\mathrm{BL}^2 = 0.14\,\mathrm{Tm}^2$ in the field of a permanent magnet, a plastic scintillator time-of-flight system, and a threshold aerogel Cerenkov counter for *e/p* discrimination. It has operated onboard the shuttle Discovery during a 10 days flight (STS-91) in June 1998. The orbit was at geodesic altitudes between 370-390 km with an inclination of 51.7° in the GTOD reference frame. The SAA region was excluded for this analysis. More details on the detector performances, proton selection and background estimation can be found in [(Alcaraz, 2000)] and references therein. A comparison of the AMS FoV, including the finite detector acceptance, with the coverages provided by satellite and balloon-borne detectors can be found in [(Fiandrini, 2001)]. The minimum mirror field encountered along the AMS orbit was $B_m = 0.225\ G$, which impose an upper limit for the FoV in the (α_0, L) space. Since the particles which are mirroring above AMS altitude cannot be observed, particles with large equatorial pitch angles can only be observed at very low L values (L≤1.2). At larger L, only particles with a smaller α_0 can be observed. Because of the fixed flight attitudes, the azimuthal β_0 coverage in the local magnetic reference frame ($\hat{z}$=$\hat{B}$, $\hat{x}$=$(\widehat{\boldsymbol{\nabla} B})_\perp$, $\hat{y}$=$\hat{z} \times \hat{x}$) was not complete.

3 Under-cutoff Proton Fluxes

All protons detected in equatorial regions ($\theta_m \leq 17^o$) outside the SAA in the Earth's magnetic field were traced us-

ing a 4^{th} order Runge Kutta method with adaptive step-size. The equation of motion was solved numerically and a particle was classified as trapped if its trajectory reached an altitude of 40 km, taken as the dense atmosphere limit, before its detection in AMS. Although satisfactory in most cases, this approach is less stable when the particle rigidity falls in the penumbra region, close to the cutoff value. In this case, the trajectories become chaotic and small uncertainties in the reconstructed rigidity and in the B field can lead to a misclassification[1]. The total time spent by each particle above the atmosphere before and after detection, the residence times T_f, of the traced under-cutoff particles are computed. The residence time distribution as a function of the kinetic energy is shown in Fig. 1. The proton residence times do

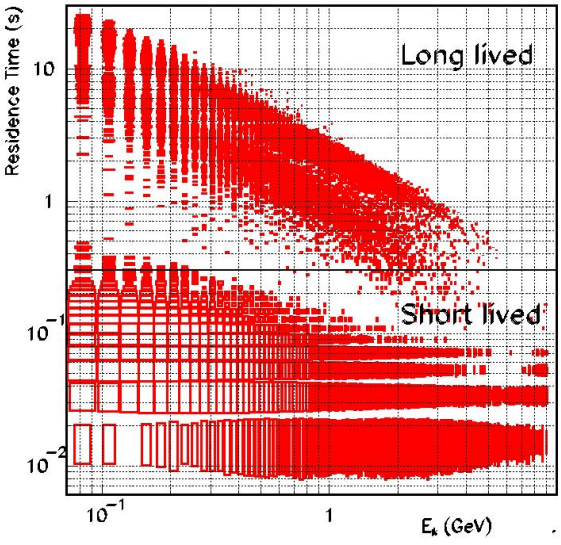

Fig. 1. Residence time vs kinetic energy for protons with $\theta_m \leq 17^o$

not exceed $\sim$ 30 s, with 50% of protons having a $T_f < 0.3$ s independent of their energy, referred to as the *short-lived* populations in Alcaraz (2000) but based on the flight time distribution, i.e. the time spent between detection and impact with the atmosphere. The geographical location where the trajectories intercept the atmosphere determine the protons *production* and *impact* points; they are localized in Fig. 2 for long lived (red/blue) and for short lived (yellow). A scaling law, $T_f \approx E^{-2}$, is observed for the protons *long-lived* which are present mostly under 6 GeV.

It is not practical to apply the tracing technique for each detectd proton of the large statistical sample O(10^6). Therefore, to reject the cosmic component of the measured proton fluxes, we defined an effective cutoff R_{eff} using a modified

[1]The validity of the adiabatic approach requires the smallness parameter $\varepsilon = \rho/R$ to be small, ρ being the equatorial Larmor radius of a particle and R the field radius of curvature at equator. A critical value exists, above which motion becomes chaotic and the adiabatic approach is no longer valid. In [(Il'in, 1986)] limits can be found for this parameter, if $\varepsilon \geq 0.1$ the motion becomes cahotic. The AMS data are consistent with this limit even though they are high energy particles.

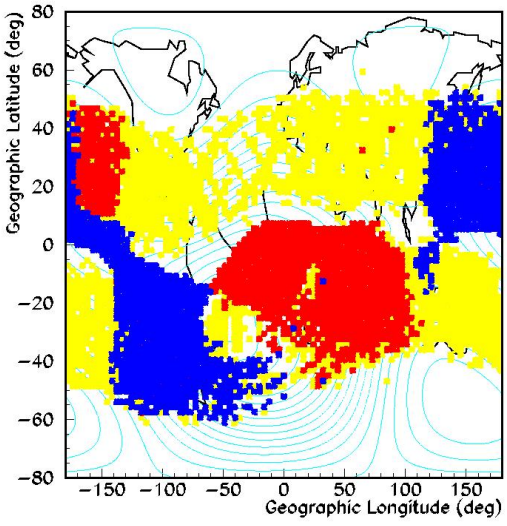

Fig. 2. Geographical positions of production and impact points with the atmosphere. Yellow bands show the distribution for short lived protons, red/blue bands show the production/impact distribution for long lived ($\theta_m \leq 17^o$).

Stormer cutoff estimated from the dipole momentum of the real magnetic field and taking into account the rigidity resolution of the detector. Magnetic latitudes above 50^o were rejected to minimize the possible contamination from the cosmic component.

4 Interpretation with an Adiabatic Approach

An original interpretation of the observed feature for electrons and positrons and their complementary structure was given in [(Fiandrini, 2001)] in terms of adiabatic invariants. All the results valid in this approach for positively charged particles, apply here for protons. The proton sample analyzed in the proton paper covers a larger range in rigidity than reported previously for positrons [(Fiandrini, 2001)]. The behaviour observed in the under-cutoff protons data is explained in terms of the geometry of drift shells crossed by the AMS along the shuttle orbit, and in particular by the fact that all the shells evolve partially in the atmosphere. The residence times depend on the altitudes of the mirror points during particle trajectory: particles whose mirror points lie mostly below the atmosphere are dominated by the bouncing period (T_b) while the others are dominated by the drifting period ($T_d \gg T_b$).

The impact/production points correspond to the intersection of the shell surfaces with the atmosphere. The yellow bands in Fig. 3, corresponding to shells with $\mathrm{B_m} \geq 0.48\,\mathrm{L}^{0.41}$ G, are consistent with the extrapolated impact/production points of the AMS traced short-lived particles. For the long-lived component the extrapolated impact/production points are consistent with the blue region in Fig. 3 corresponding to shell with $\mathrm{B_m} \leq 0.48\,\mathrm{L}^{0.41}$ G.

We use the rigidity R, L and α_0 to describe the behaviour

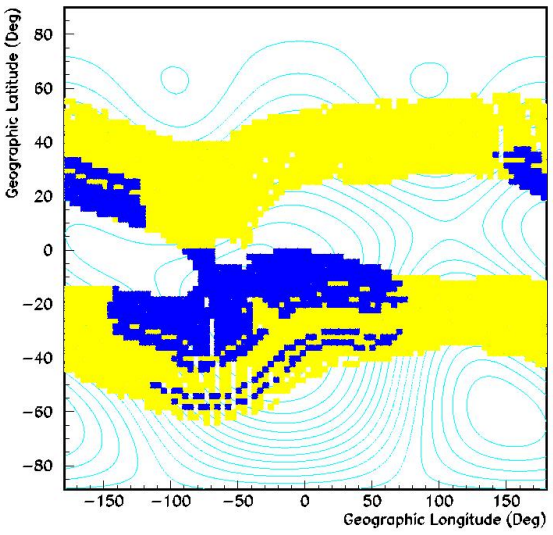

Fig. 3. Distribution of intersection points with atmosphere for the drift shells crossed by AMS. Yellow region corresponds to shells with $B_m \geq 0.48\,L^{0.41}$ G, blue one to $B_m \leq 0.48\,L^{0.41}$ G

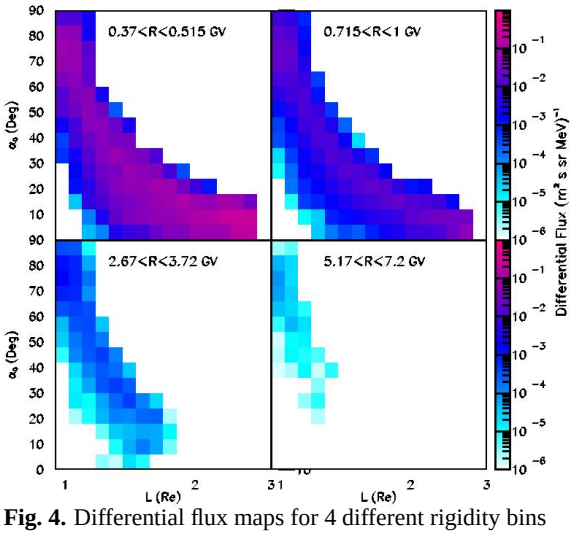

Fig. 4. Differential flux maps for 4 different rigidity bins

of under cutoff fluxes. Flux maps were built using a linear binning in α_0 and logarithmic variable size for L and R bins to optimize statistics for each bin according to Table 1. The 2-dimensional flux maps in (L, α_0) at constant R give the distribution of particle populations at the altitude of AMS. The differential flux maps in four rigidity bins are shown in Fig. 4 with an observed intensity smaller than $1\ [m^2 ssr MV]^{-1}$, well below the expected intensity for a trapped component. The effect of the rigidity cutoff R_c is clearly observed: on a given shell only particles with R $\leq R_c$ are allowed to populate the shell, therefore only low energy particles can populate higher shells. A rapid decay of the intensity is observed as the rigidity increases. At the altitudes of AMS, an important parameter is the directional distribution of the particles. The intrinsic azimuthal β angle allows a separation between particles coming from the local magnetic east and west. According to the definition, particles coming from west have always $\beta \leq 0$, while those coming from east $\beta \geq 0$. Fluxes integrated over two rigidity intervals separating $\beta < 0$ and $\beta > 0$ components, are shown in Fig. 5. In A) and B) the fluxes integrated over 0.37≤R≤3.7 GV for $\beta > 0$ and $\beta < 0$, respectively, are shown, while in C) and D) the integration is in the interval 3.7≤R≤10 GV. The distributions integrated over α_o and L are shown in Fig. 6 A) and B), respectively. The East-West flux asymmetries A, defined as $(J_{\beta<0} - J_{\beta>0})/(J_{\beta<0} + J_{\beta>0})$, in the two rigidity bins as function of L and α_o are shown in Fig. 6 C) and D), respectively. The flux fractions of the East/West components in the two rigidity bins are shown in Fig. 7. At low altitudes the high energy trapped proton flux (3.7≤R≤10 GV) appears to be strongly anisotropic. Moreover, the flux asymmetry shows a marked dependence on the L shell and α_o for the high rigidity component, with a smooth and steep transition from Eastward flux at low L to a completely Westward flux at higher shells, the two components at the same level for L$\simeq$ 1.2 R_e. At low L values the asymmetry arises from the fact that Eastward particles have always the guiding centres below the detection position and therefore are removed from the belts by the atmospheric interactions, due to the scale length of the proton gyroradius comparable with the shuttle altitude for very high energies. At higher L, trajectories having the guiding centre much above the observation point are not allowed due to geomagnetic cutoff effects, and therefore only Eastward particles are present. A priori, a comparison with the AP8 or INP models for the stably trapped component is not possible since the SAA data were excluded in this analysis, however in Fig. 8 a comparison between AMS proton fluxes and AP8 for locally mirroring particle ($\alpha_0 \geq 70$) and $L = 1.2$ is shown. A computation for the albedo component taken from (Ray, 1962) is also shown. Different groups have attempted to explain the observed AMS under cutoff proton spectra [(Derome, 2000),(Zuccon, 2001)]. For exam-

	N bin	Limit	Bin Width
R	9	0.37-10 GV	0.159 (log.)
L	16	0.95-3	0.031 (log.)
α_0	15	$0^o - 90^o$	6^o (lin.)

Table 1. Bin limits used for AMS data binning

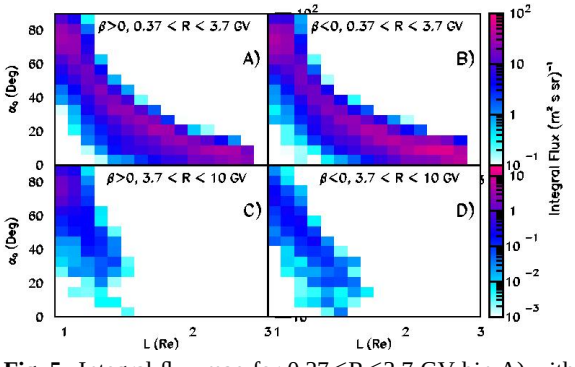

Fig. 5. Integral flux map for 0.37≤R≤3.7 GV bin A) with $\beta \geq 0$ and B) $\beta \leq 0$, and for 3.7≤R≤10 GV bin C) with $\beta \geq 0$ and D) $\beta \leq 0$

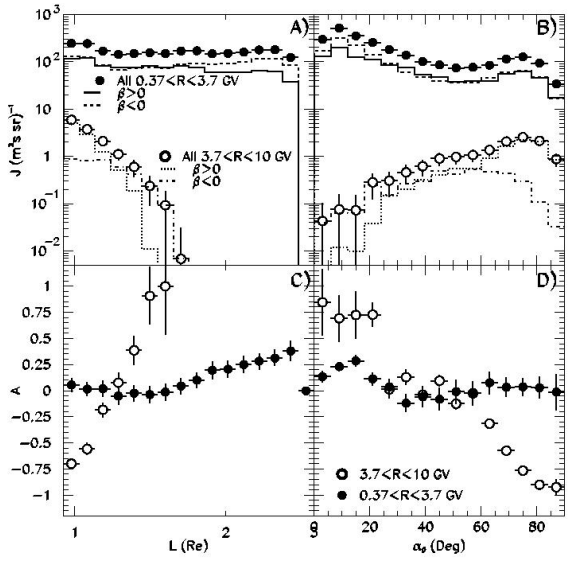

Fig. 6. Integral flux and asymmetries as function of α_0 (B,D) and of L (A,C) for protons

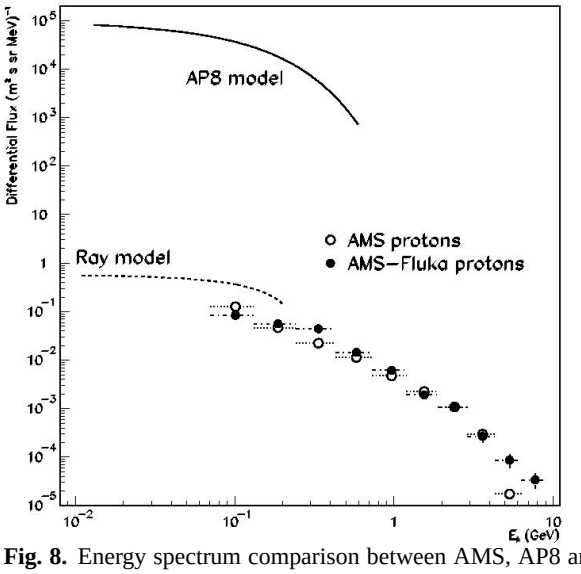

Fig. 8. Energy spectrum comparison between AMS, AP8 and MC data for particles with $\alpha_0 \geq 70^o$ and L=1.2

ple in [(Zuccon, 2001)], the albedo component is completely explained by secondary production from interactions at the intersections of drift shells with atmosphere. The spectra obtained from secondary production [(Zuccon, 2001)], shown in Fig. 8 superimposed to data, agree well with the observed flux.

5 Conclusion

The AMS data indicates clearly the existence of albedo protons radiation belts underneath the Inner Van Allen belts for particle rigidities of several GV. The measured fluxes are not stably trapped since the corresponding drift shells are not closed over the SAA region. Anisotropies are observed at rigidities above 3.7 GV due to the gyroradius and the relative correction to the guiding center approximation and geomagnetic cutoff effects. The interaction of primary cosmic rays and inner radiation belt protons with atmospheric nuclei in the regions of shell intersection with atmosphere are a natural mechanism for the production of the observed secondary protons.

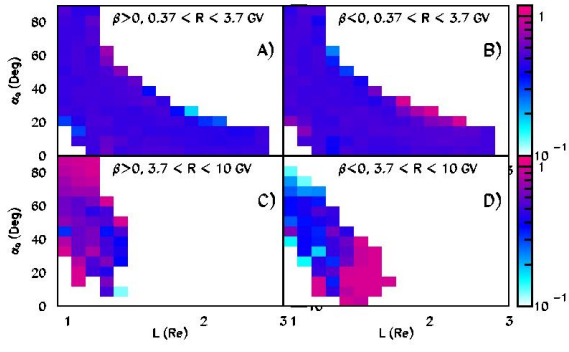

Fig. 7. East/West fractions between 0.37≤R≤10 GV, for $\beta > 0$ and $\beta < 0$

Acknowledgements. We gratefully acknowledge the contribution of our collegues in AMS. We greatly benefit of the software libraries (UNILIB,SPENVIS) developed in the context of the Trapped Radiation ENvironment Development (TREND) project for ESTEC.

References

J. Alcaraz et al., Phys. Lett. B, 472, p. 215, 2000.

L. Derome et al., Phys. Lett. B, 489, p. 1-8, 2000.

Fiandrini et al., Leptons with $E \geq 200$ MeV trapped in the Earth's radiation belts, Proc. of ICRC, 2001

Getselev I.V. et al., Model of spatial-energetic distribution of charged particles (protons and electrons) fluxes in the Earth's radiation belts, INP MSU Preprint MGU-91-37/241, 1991 (in Russian)

Hilton H. , L parameter: a new approximation, J. Geophys. Res., 28, 6952, 1971.

IGRF, http://nssdc.gsfc.nasa.gov/space/model/magnetos/igrf.html

Il'in V.D. et al., Stochastic instability of charged particles in a magnetic trap, Cosmic Res., 24, 69-76, 1986

McIlwain C.E., Coordinate for mapping the distribution of magnetically trapped particles, J. Geophys. Res., 66,3681, 1961.

Ray E.C. , Re-entrant Cosmic Ray Albedo, J. Geophys. Res., 67, 3289, 1962.

Sawyer, D.M., Vette J.I., AP-8 Trapped Proton environment, NSSDC/WDC-A-RS 76-06, 1976

TREND project, http://www.magnet.oma.be/home/trend-/trend.html, http://www.magnet.oma.be/unilib.html

Zuccon et al., A Montecarlo simulation of the interactions of cosmic rays with the atmosphere, Proc. of ICRC, 2001